Published in final edited form as:

Nat Struct Mol Biol. 2010 August ; 17(8): 971–975. doi:10.1038/nsmb.1847.

Structural Basis for the Transcriptional Regulation of Membrane Lipid Homeostasis

Darcie J. Miller[1], **Yong-Mei Zhang**[2,3], **Chitra Subramanian**[2], **Charles O. Rock**[2], and **Stephen W. White**[1,4]

[1]Department of Structural Biology, St. Jude Children's Research Hospital, 262 Danny Thomas Place, Memphis, TN 38105.

[2]Department of Infectious Diseases, St. Jude Children's Research Hospital, 262 Danny Thomas Place, Memphis, TN 38105.

Abstract

DesT is a transcriptional repressor that regulates the genes which control the unsaturated:saturated fatty acid ratio available for membrane lipid synthesis. DesT bound to unsaturated acyl-CoA has a high affinity for its cognate palindromic DNA-binding site, whereas DesT bound to saturated acyl-CoA does not bind to this site. Structural analyses of the DesT–oleoyl-CoA–DNA and DesT–palmitoyl-CoA complexes reveal that acyl chain shape directly influences the packing of hydrophobic core residues within the DesT ligand-binding domain. These changes are propagated to the paired DNA-binding domains via conformational changes to modulate DNA binding. These structural interpretations are supported by the *in vitro* and *in vivo* characterization of site-directed mutants. The regulation of DesT by the unsaturated:saturated ratio of acyl chains rather than the concentration of a single ligand is a paradigm for understanding transcriptional regulation of membrane lipid homeostasis.

The ability of bacteria to adjust their membrane lipid composition to adapt to the environment is vital to bacterial physiology1. Control over the membrane viscosity is primarily determined by the fatty acid composition of the phospholipids. The remarkable ability of bacteria to modify their membrane fatty acid composition in response to challenges, such as temperature, osmolarity, pH and exogenous fatty acids, is termed homeoviscous adaptation1,2. In Gram-negative bacteria, adaptation is achieved by altering the ratio of unsaturated (UFA) to saturated (SFA) fatty acids delivered to the glycerol-

---

[4]Correspondence should be addressed to (stephen.white@stjude.org)..

[3]Present address: Department of Biochemistry and Molecular Biology, Medical University of South Carolina, 173 Ashley Ave., Charleston, SC 29425.

AUTHOR CONTRIBUTIONS D.J.M. and S.W.W. designed and executed the crystallography experiments. Y.M.Z., C.S. and C.O.R. designed and executed the biochemical and genetic experiments. All authors participated in writing the manuscript.

COMPETING INTERESTS STATEMENT The authors declare no competing financial interests.

METHODS Methods and any associated references are available in the online version of the paper at http://www.nature.com/nsmb/.

Note: Supplementary information is available on the Nature Structural & Molecular Biology website.

Accession codes. Protein Data Bank: coordinates and structure factors for the DesT–18:1Δ9-CoA–DNA, DesT–16:0-CoA and DNAPP complexes are deposited with accession codes of 3LSP, 3LSJ and 3LSR respectively.

phosphate acyltransferases, and this identifies the *de novo* fatty acid biosynthetic pathway as a focal point for the regulatory events that control membrane homeostasis. In *Escherichia coli*, the UFA:SFA ratio is regulated by the FabR transcriptional repressor that regulates the expression of the two genes essential for UFA synthesis, *fabA* and *fabB*3. The binding of FabR to its cognate DNA palindrome located within the promoters of the *fabA and fabB* genes requires the presence of an unsaturated acyl-acyl carrier protein (acyl-ACP) or acyl-CoA, and binding is antagonized by saturated acyl-ACP or acyl-CoA4. Thus, FabR is an unusual transcriptional regulator that adjusts gene expression in response to the UFA:SFA ratio rather than to the simple presence/absence of a specific regulatory ligand.

DesT is a transcriptional regulator that is the *Pseudomonas aeruginosa* homolog of *E. coli* FabR5. In addition to modulating the expression of the *P. aeruginosa fabAB* operon6, DesT also controls the expression of the *desCB* operon encoding an oxygen-dependent acyl-CoA Δ9-desaturase that converts SFA-CoA (16:0- or 18:0-CoA) to Δ9-UFA-CoA (16:1Δ9- or 18:1Δ9-CoA)5. *P. aeruginosa* readily converts extracellular fatty acids to their respective CoA thioesters and incorporates them into membrane phospholipids5. *P. aeruginosa* phospholipids normally contain a high proportion of UFA, and abundant extracellular SFA levels have the potential to perturb membrane homeostasis. SFA-CoAs induce *desCB* expression by releasing DesT from DNA, whereas UFA-CoAs promote the binding of DesT to its cognate DNA and repress desaturase expression7. DesT binds UFA- and SFA-CoAs with approximately equal affinity suggesting that, in a similar fashion to FabR, DesT is an atypical bacterial repressor that senses the UFA:SFA ratio of the acyl-CoA pool rather than the concentration of an acyl-CoA ligand7. In this study, the crystal structures of the DesT–UFA-CoA–DNA and DesT–SFA-CoA complexes were determined, and site-directed mutants were characterized biochemically and *in vivo* to understand the mechanism by which fatty acids that differ by only a single double bond modulate DesT DNA binding.

RESULTS

The Overall Structure of DesT

The crystal structures of the DesT–UFA-CoA–DNA and DesT–SFA-CoA complexes were determined, and the data collection and refinement statistics are provided in Table 1. Detailed structural descriptions are provided in Supplementary Results and representative electron density maps are shown in Supplementary Fig. 1. Briefly, the fold of each protomer and the dimeric arrangement are similar to those of TetR8,9, QacR10 and EthR11,12, three members of the TetR repressor family. DesT forms a parallel dimer with each protomer composed of nine α-helices folded into two discrete domains (Fig. 1a). The three N-terminal α-helices create the DNA-binding domain, and the six C-terminal helices create the ligand-binding domain. In the latter domain, helices α4, α5, α7, α8 and α9 are arranged in an antiparallel bundle with helix α6 diagonally crossing the ‘top’ of the bundle forming a platform for the DNA-binding domain. Within the dimer, hydrophobic interactions between the paired helices α8 and α9 that cross at the interface of the ligand-binding domains create a central 4-helical bundle. TetR-like proteins are usually described as existing in two conformations: the DNA-bound ‘uninduced’ form and the ligand-bound ‘induced’ form that does not bind DNA13. This description does not apply to DesT because its function is not

determined by the simple presence or absence of ligand. DesT has a defined structural pathway to relay ligand shape to the DNA-binding domains some 40 Å away, and is therefore better described in allosteric terms. The DesT–oleoyl-CoA–DNA ternary complex corresponds to the relaxed (R) state and the DesT–palmitoyl-CoA binary complex represents the tense (T) state.

DesT–18:1-CoA–DNA Complex

DesT–oleoyl-CoA is bound to a 30 base duplex DNA containing the 18 base-pair pseudo-palindromic *desCB* promoter sequence7 (AGTgAACgcttGTTgACT) (Fig. 1a). The DNA-binding N-terminal domain contains a helix-turn-helix motif composed of α2, loop L2-3 and α3 (Fig. 1b). Helix α2 acts as the 'platform' helix spanning the cognate major groove and α3 acts as the 'recognition' helix penetrating the major groove. The N-terminus of α1 binds across the adjacent minor groove. It has been noted that the N-terminus of α4 within the ligand-binding domain contributes to the binding of DNA in the TetR-repressor family, with the helix dipole and a conserved lysine residue (Lys48 in TetR) engaging the DNA backbone14. However, in DesT, the N-terminus of α4 is 7 Å from the DNA and lacks this conserved lysine. The platform helix α2 specifically engages chain 2, and the recognition helix α3 makes extensive interactions with both DNA chains (Supplementary Fig. 2a). The DesT–DNA interface mainly involves the phosphates of the DNA backbone, except for specific interactions with a pair of guanine bases within each half site. Specifically, the guanidinium groups of Arg36 and Arg51 interact with +3 and −8 guanine bases (with respect to the dyad axis of the cognate sequence) within chains 2 and 1, respectively (Supplementary Fig. 2a). In the crystal structure, the DNA binds 50:50 in both orientations reflecting DesT recognition of the sugar-phosphate backbone and the two palindromic guanines. A crystal structure (not shown) using a fully palindromic sequence confirms this mode of recognition (DNAPP in Table 1).

The DNA is bent by 3.3° toward the protein (Fig. 1a) and the B-DNA helix is slightly deformed at the recognition site (Supplementary Fig. 2b, Supplementary Table 1); the major groove is widened from 11.7 Å to 12.1–13.4 Å and the helical repeat increases from 34 Å to 36 Å, slightly unwinding the DNA.

The L-shaped oleoyl (18:1) chain of the ligand is buried within the hydrophobic interior of the DesT ligand binding domain to become an integral component of the hydrophobic core (Fig. 1c, Supplementary Fig. 3a). The CoA moiety was not visible in the electron density map and is presumably disordered (Supplementary Fig. 1a). The kink in the 18:1 chain at the *cis*-9 double bond directs the chain towards the periphery where the distal end projects between α4 and α7, and phenylalanines 71, 96, 107 and 166 together with Leu169 form a phenylalanine-rich cluster directly above the kink and below α6. The paired C-termini of α6 and α6′ loosely associate via stacking interactions between the side chains of Arg112 and Arg122′, and an edge-to-face interaction between Tyr115 and Pro170′ at the C-terminus of α8 (Supplementary Fig. 3a).

DesT–16:0-CoA Complex

In the DesT–16:0-CoA binary complex, the entire 16:0-CoA molecule is visible. The C-terminus of DesT is well ordered and reveals the adenine ring interactions. The adenine ring stacks between Ile199 and His205′ adjacent to Trp204′, and the N1 and N6 nitrogen atoms form hydrogen bonds with the amide nitrogen of His205′ and the carbonyl oxygen of His203′, respectively. The entrance to the ligand binding pocket is largely unaffected by the ligand swap because the first 7 carbons of the 16:0 chain form similar interactions to those of the oleoyl chain. However, the tail of the 16:0 linear chain inserts directly into the hydrophobic core and creates a new 9 Å hydrophobic pocket, reminiscent of the ligand-binding hydrophobic pocket in EthR11,12. Most notably, the acyl chain penetrates the phenyalanine-rich cluster below α6 and these residues adjust their positions to accommodate the ligand (Fig. 1d; Supplementary Fig. 3b). These rearrangements result in three conformational changes. First, helices α4 and α7 pack closer together, and a slight bend is induced in α4 due to the local unwinding of residues 68 to 71. This unwinding is associated with the movement of Phe71 and is stabilized by a hydrogen bond between the side chain of Thr70 and the carbonyl oxygen of Glu66. Second, the C-terminus of α6, loop L6-7 and the N-terminus of α7 engage loop L8-9 which extends across the interface and becomes ordered. L8-9 contains five proline residues and appears to act as a clamp that specifically stabilizes the T state conformation. Finally, and most significantly, the C-termini of the paired α6 helices slide closer together by one turn (~4.4 Å), and this new location is stabilized by new interactions centered on Tyr115 (Supplementary Fig. 3b). The side chain engages a hydrophobic pocket comprising Leu108′, Ala111′, Arg112′, Tyr115′, Leu169′, Pro170′ and Ile173′; the main chain carbonyl oxygen becomes hydrogen bonded to the side chain of Arg112′; and the guanidinium group of Arg129 swaps hydrogen-bonding partners from the OH of Tyr115 to the side chain of Gln114.

The core four-helix bundle of the dimer in most TetR family members is a stable substructure14, and this is also true in DesT. Superposition of the paired α8/α9 and α8′/α9′ helices in the R- and T-states clearly shows the three conformational changes described above (Fig. 2a). It also reveals the substantial relative movements of the DNA-binding domains in the T form away from their optimal DNA-binding orientations in the R form (Fig. 2b). The recognition helices α3 and α3′ rotate by some 5°, and their center-to-center distance increases from the required DNA binding distance of 36.7 Å to 41.9 Å. These movements are comparable to those observed in TetR where the distance between the recognition helices increases from 36.6 Å to 39.6 Å8.

Activities of DesT Mutants

The structures suggest specific roles for key residues in transmitting the ligand shape information to the DNA-binding domain (Fig. 2c). Tyr115 at the C-terminus of α6 is important in the T state to fix the orientation of this helix at the dimer interface. We confirmed this by showing that DesT Y115A, unlike DesT (Table 2; Fig. 2d), constitutively binds DNA regardless of the structure of the bound acyl-CoA (Table 2; Fig. 2e). DesT Y115A binds both 16:0-CoA and 16:1Δ9-CoA with similar affinities (Table 2), illustrating that this substantial modification of its DNA binding properties did not simply arise from an inability to bind SFA-CoA. The side chain of Phe71 contacts the ligand to introduce a bend

into α4 in the T state, and DesT F71A also exhibits constitutive DNA binding (Table 2). Phe96 and Leu169 are two other side chains that stabilize the hydrophobic core of the T state, and DesT F96A and DesT L169A bind UFA- and SFA-CoAs equally well and constitutively bind DNA (Table 2). We note that F71A, F96A and L169A will each leave voids in the hydrophobic core that could be accessed by the flexible 16:0 acyl chain and contribute to the failure of 16:0 to stabilize the T state.

Phe166 is exquisitely positioned to detect the conformation at the 9-position of the acyl chain where the *cis* double bond is located (Fig. 2c). This role directly reflects the physiological function of DesT, which is to control the expression of a desaturase that introduces a *cis* double bond at the 9-position of the acyl chain7. DesT F166A binds both acyl-CoA ligands, but fails to bind DNA under any condition (Table 2; Fig. 2f), and is therefore locked into the T state regardless of fatty acid structure. Phe166 sits directly below α6, and stabilizes its orientation in the R state (Fig. 1c, Supplementary Fig. 3a). The lack of the aromatic side chain prevents the transmission of ligand shape information to α6 leaving the F166A mutant locked in the T state.

These *in vitro* results were corroborated *in vivo* by analyzing *desCB* gene expression in strain PA0482 (Δ*desT*) expressing either DesT, or the Y115A or F166A mutants from a plasmid (Fig. 2g). The expression of the wild-type DesT illustrates the normal activity of the protein. In the absence of an exogenous ligand, DesT has repressor activity *in vivo* due to endogenous ligands that establish an equilibrium between the T and R states. The addition of 16:1Δ9 to the medium represses *desCB* transcription by stabilizing the R state, whereas the addition of 16:0 to the medium activates transcription through the stabilization of the T state (Fig. 2g). DesT Y115A is permanently locked in the R state *in vitro* (Fig. 2e), and accordingly, *desCB* transcription is repressed regardless of the fatty acid presented to the cells (Fig. 2g). On the other hand, DesT F166A is locked in the T state (Fig. 2f), and there is no repression of *desCB* transcription regardless of the fatty acid in the medium. Cells expressing DesT F166A have *desCB* mRNA levels that are the same as in cells harboring an empty vector indicating that the F166A mutant cannot repress *desCB in vivo* (Fig. 2g).

DISCUSSION

DesT is a paradigm for lipid transcriptional regulators that sense the composition, rather than only the concentration, of a ligand pool. The TetR-like regulators are on-off control switches that respond to the concentration of a related set of ligand structures, which they sense with high affinity8,10,11,15-17. DesT has a similar architecture to the TetR-like proteins and undergoes similar structural transitions centered on the paired α6 helices, and it is clearly a member of this large family of transcriptional regulators. However, the ability of DesT to differentially respond to alternate ligand shapes is a unique property that allows it to function as a rheostat in membrane lipid homeostasis. The allosteric conformational changes that regulate DNA binding begin within the phenylalanine-rich hydrophobic cluster lying beneath helix α6 within the ligand binding domain. Phe71, Phe96, Phe166 and L169 sense which ligand is bound and mold the hydrophobic core to create the specifically shaped cavities to accommodate ligand structure. This reorganization of the hydrophobic core directly impacts the position and orientation of the adjacent helix α6, and the translocation

of α6 results in the coordinated movement of the tethered helices α5 and α4. Helices α4 and α6 are shared by the DNA- and ligand-binding domains, and their movements in response to ligand shape adjust the relative positioning of the paired DNA-binding domains to control their interaction with DNA. In the T state, the dimeric structure is preferentially stabilized by the tighter association of the paired α6 helices that involves multiple interactions centered on Tyr115, and the formation of the L8-9 interfacial clamp. At the same time, the protomer can be considered as being destabilized by a partial unwinding and bending of helix α4 caused by the rotation of the Phe71 side chain. The opposite is true in the R state where the α6 helices only marginally interact and α4 is not distorted.

The UFA:SFA ratio in phospholipids is a key determinant of membrane biophysical properties1,2, and the ability of DesT to monitor this ratio and appropriately tune gene expression to direct cellular fatty acid metabolism is an elegant mechanism that ensures the phospholipid biosynthetic pathway will be supplied with a balanced fatty acid composition. A key feature of this mechanism is that it allows DesT to appropriately adjust gene expression even when the intracellular concentration of acyl-CoA is saturating the transcription factor. The existence of compositional sensors that regulate lipid metabolism may be widespread in nature. *E. coli* FabR is a close relative of DesT that regulates *fabA and fabB* expression based on the UFA:SFA ratio4, and *Streptococcus pneumoniae* FabT regulates fatty acid synthesis based on the chain-length composition of the acyl-ACP pool18. The DesT structural paradigm may apply to other regulators of lipid metabolism where metabolic end-products and intermediates are abundant, and the biophysical properties of the mixture are more important to control than the concentration of a specific molecule.

ONLINE METHODS

Expression and purification of DesT

Recombinant DesT proteins with a C-terminal His-tag were purified7. The DesT mutants were generated by PCR based mutagenesis by introducing the base changes for the amino acids using the Quikchange mutagenesis kit (Stratagene Inc.). The identity of the constructs was confirmed by DNA sequencing. The stability of DesT and its mutant derivatives were compared using the SYPRO Orange dye-binding assay19. The transition temperatures for protein unfolding were: DesT, 63°C; Y115A, 55°C; F166A, 61°C; F96A, 52°C; F71A, 56°C; and L169A, 56°C.

DesT regulation of *desCB* expression *in vivo*

An NcoI site was engineered into the multiple cloning site of pUC2020 and the 70-bp NcoI-BamHI fragment from pET15b was introduced to make the Pseudomonas shuttle vector pUCP20-Hy. DesT and the DesT mutants (Y115A and F166A) were cloned into pPUCP20-Hy by digesting the pET28b expression plasmids with BlpI-Klenow filled for blunt ends and NcoI to generate a 735-bp fragment that was inserted into pUCP20-Hy. The resulting plasmids were transformed into *P. aeruginosa* strain PAO482 (Δ*desT*)21, and the strains were grown in M9 + 0.4% glycerol minimal medium in the presence or absence of 0.1% palmitate (16:0) or pamitoleate (16:1Δ9). RNA was isolated using Ambion RNAqueous

purification kit (Ambion). The expression levels of *desB* were measured by real-time PCR5. Values were compared using the C_T method, where the amount of *desB* cDNA ($2^{-\Delta\Delta CT}$) was normalized to *rpoD* (ΔC_T) and comparisons were made using $\Delta\Delta C_T$ method.

Determination of the affinities of DesT for UFA- and SFA-CoA

Direct binding of acyl-CoAs to DesT was measured by fluorescence spectroscopy on a Fluorolog-3 spectrofluorimeter (Horiba Jobin Yvon)7. Intrinsic protein fluorescence was measured with excitation at 280 nm and emission at 340 nm (slits set at 5 nm). The concentration of DesT was 4 μM in 20 mM Tris-HCl buffer, pH 7.5, and acyl-CoAs were titrated in 2-μl increments from stock solutions. The data were not corrected for the inner filter effect due to the low absorbance (0.008 average) of acyl-CoA in the experiments22. Each curve was corrected for the nominal fluorescence of acyl-CoA and fitted to one site specific binding equation $Y=Bmax\times X/(Kd + X)$, where Y is the fluorescent signal of the protein and X is the acyl-CoA concentration. Examples of the fluorescence titration experiments are provided in Supplementary Fig. 4.

Gel mobility shift assays

Protein-DNA gel retardation assays were performed using the 32P-labeled *desCB* oligo probe as described6,7. Assays contained, 20 mM Tris pH 7.5, 50 mM NaCl, 1 mM DTT, 1 mM EDTA, 300 μg/ml BSA, 0.05 unit poly[d(I-C)], and [32P]DNA (2500 cpm, approximately 1×10^{-11} M) in 20 μl in the presence of 0, 1 or 10 μM 16:0-CoA or 16:1Δ9-CoA. The mixture was incubated at 22°C for 30 min, and loaded onto a 6% DNA retardation gel. The gels were autoradiographed against a phosphor storage screen and quantified with a Typhoon 9200 (GE Healthcare) using ImageQuant 5.2 software (Molecular Dynamics). DesT binding was indicated by the conversion of the free DNA probe to the DesT–DNA complex. The apparent Kds were determined as described above. Examples of the gel shift experiments are shown in Supplementary Fig. 4.

Crystallization, Structure Determination and Model Quality

P. aeruginosa DesT selenomethionine protein was crystallized in the presence of an oligonucleotide corresponding to the *desCB* promoter (30mer duplex with a 5′ T overhang, 5′-TTACATCAGTGAACGCTTGTTGACTCGATTG) and 18:1Δ9-CoA at 18°C by sitting drop vapor diffusion under mineral oil. The 4.5 μl drop contained 2 μl DesT-ligand mixture (0.3 mM protein, 0.3 mM oligo, 0.3 mM 18:1Δ9-CoA), 2 μl mother liquor (ML) (0.1 M MES pH 7.0, 9% PEG 20K), and 0.5 μl 1 M ammonium sulfate. Crystals were cryo-preserved in 30% glycerol/70% ML. SAD data at the Se peak (0.9792 Å) were collected at the SER-CAT ID beamline to 3 Å. The substructure was determined by HySS23. An initial model of the protein component was generated using Resolve24, and this served as the Phaser25 molecular replacement model for the ternary complex 2.65 Å data collected at 1.0 Å on the SER-CAT BM beamline. The crystals belong to space group $I4_1$ with one protomer and one DNA strand in the asymmetric unit. The DesT dimer/DNA duplex assembly is generated by 2-fold symmetry. The final model lacks residues 1–3, 175–182 (the L8-9 loop), C-terminal residues 206–209, and tag residues 210–226, and only the buried acyl chain of

18:1Δ9-CoA and DNA bases 5–27 were visible. Ramachandran statistics show that 94.7% and 5.3% of the residues are in the preferred and allowed regions, respectively.

DesT was crystallized in the presence of 16:0-CoA at 18°C by the sitting drop method. The ML contained 0.1 M HEPES pH 7.5, 0.1 M magnesium acetate, and 15% PEG 4K. The drop contained 2 μl DesT-ligand mixture (20 mg/ml protein, 0.9 mM 16:0-CoA) and 2 μl ML. Crystals were cryo-preserved in 15% glycerol/85% ML. A 2.3 Å dataset was collected at 1.0 Å on the SER-CAT BM beamline, and the DesT–18:1Δ9-CoA–DNA model was used for molecular replacement with Phaser. The crystals belong to space group $P2_1$ with the dimer in the asymmetric unit. The final model lacks residue 1, C-terminal residue 209, tag residues 210–226, residues in the L4-5 loop; residues 83–84 in chain A and 83–85 in chain B. Ramachandran statistics show that 98.5% and 1.5% of the residues are in the preferred and allowed regions, respectively.

Model building was performed using COOT26. Structure refinement was performed using Refmac27 and CNS28, and 5% of the data was sequestered for the calculation of Rfree. Structural figures were generated with PyMol29, and ligand cavity volumes were calculated with Castp30 and HOLLOW31. The final structure statistics were calculated using PROCHECK32. The analysis of the DNA conformation shown in Supplementary Fig. 2b and Supplementary Table 1 was performed using 3DNA33.

Supplementary Material

Refer to Web version on PubMed Central for supplementary material.

ACKNOWLEDGMENTS

This work was supported by National Institutes of Health Grant GM34496 (C.O.R.), Cancer Center (CORE) Support Grant CA21765, and the American Lebanese Syrian Associated Charities. Data were collected at Southeast Regional Collaborative Access Team (SER-CAT) 22-ID and 22-BM beamlines at the Advanced Photon Source, Argonne National Laboratory. Supporting institutions may be found at www.ser-cat.org/members.html. Use of the Advanced Photon Source was supported by the U. S. Department of Energy, Office of Science, Office of Basic Energy Sciences, under Contract No. W -31 -109 Eng 38. We thank Mathew Frank for his technical assistance, and the St. Jude Protein Production Facility for the expression and purification of DesT and its selenomethionine-labeled derivative.

REFERENCES

1. Zhang Y-M, Rock CO. Membrane lipid homeostasis in bacteria. Nat. Rev. Microbiol. 2008; 6:222–233. [PubMed: 18264115]
2. Cronan JE Jr. Gelmann EP. Physical properties of membrane lipids: biological relevance and regulation. Bacteriol. Rev. 1975; 39:232–256. [PubMed: 1100043]
3. Zhang Y-M, Marrakchi H, Rock CO. The FabR (YijC) transcription factor regulates unsaturated fatty acid biosynthesis in *Escherichia coli*. J. Biol. Chem. 2002; 277:15558–15565. [PubMed: 11859088]
4. Zhu K, Zhang YM, Rock CO. Transcriptional regulation of membrane lipid homeostasis in *Escherichia coli*. J. Biol. Chem. 2009; 284:34880–34888. [PubMed: 19854834]
5. Zhu K, et al. Two aerobic pathways for the formation of unsaturated fatty acids in *Pseudomonas aeruginosa*. Molec. Microbiol. 2006; 60:260–273. [PubMed: 16573679]

6. Subramanian C, Zhang Y-M, Rock CO. DesT coordinates the expression of anaerobic and aerobic pathways for unsaturated fatty acid biosynthesis in *Pseudomonas aeruginosa*. J. Bacteriol. 2010; 192:280–285. [PubMed: 19880602]
7. Zhang Y-M, Zhu K, Frank MW, Rock CO. A *Pseudomonas aeruginosa* transcription factor that senses fatty acid structure. Molec. Microbiol. 2007; 66:622–632. [PubMed: 17877713]
8. Orth P, et al. Structural basis of gene regulation by the tetracycline inducible Tet repressor-operator system. Nat. Struct. Biol. 2000; 7:215–219. [PubMed: 10700280]
9. Hinrichs W, et al. Structure of the Tet repressor-tetracycline complex and regulation of antibiotic resistance. Science. 1994; 264:418–420. [PubMed: 8153629]
10. Schumacher MA, et al. Structural mechanisms of QacR induction and multidrug recognition. Science. 2001; 294:2158–2163. [PubMed: 11739955]
11. Frénois F, et al. Structure of EthR in a ligand bound conformation reveals therapeutic perspectives against tuberculosis. Mol. Cell. 2004; 16:301–307. [PubMed: 15494316]
12. Dover LG, et al. Crystal structure of the TetR/CamR family repressor *Mycobacterium tuberculosis* EthR implicated in ethionamide resistance. J. Mol. Biol. 2004; 340:1095–1105. [PubMed: 15236969]
13. Ramos JL, et al. The TetR family of transcriptional repressors. Microbiol. Mol. Biol. Rev. 2005; 69:326–356. [PubMed: 15944459]
14. Aleksandrov A, Schuldt L, Hinrichs W, Simonson T. Tet repressor induction by tetracycline: a molecular dynamics, continuum electrostatics, and crystallographic study. J. Mol. Biol. 2008; 378:898–912. [PubMed: 18395746]
15. Gu R, et al. Crystal structure of the transcriptional regulator CmeR from *Campylobacter jejuni*. J. Mol. Biol. 2007; 372:583–593. [PubMed: 17686491]
16. Li M, et al. Crystal structure of the transcriptional regulator AcrR from *Escherichia coli*. J. Mol. Biol. 2007; 374:591–603. [PubMed: 17950313]
17. Orth P, et al. Conformational changes of the Tet repressor induced by tetracycline trapping. J. Mol. Biol. 1998; 279:439–447. [PubMed: 9642048]
18. Jerga A, Rock CO. Acyl-acyl carrier protein regulates transcription of fatty acid biosynthetic genes via the FabT repressor in *Streptococcus pneumoniae*. J. Biol. Chem. 2009; 284:15364–15368. [PubMed: 19376778]
19. Niesen FH, Berglund H, Vedadi M. The use of differential scanning fluorimetry to detect ligand interactions that promote protein stability. Nat. Protoc. 2007; 2:2212–2221. [PubMed: 17853878]
20. West SE, et al. Construction of improved *Escherichia-Pseudomonas* shuttle vectors derived from pUC18/19 and sequence of the region required for their replication in *Pseudomonas aeruginosa*. Gene. 1994; 148:81–86. [PubMed: 7926843]
21. Choi KH, Kumar A, Schweizer HP. A 10-min method for preparation of highly electrocompetent *Pseudomonas aeruginosa* cells: Application for DNA fragment transfer between chromosomes and plasmid transformation. J. Microbiol. Methods. 2005; 64:391–397. [PubMed: 15987659]
22. Lakowicz, JR. Principles of Fluorescence Spectroscopy. Springer; Singapore: 2008.
23. Grosse-Kunstleve RW, Adams PD. Substructure search procedures for macromolecular structures. Acta Crystallogr. D Biol. Crystallogr. 2003; 59:1966–1973. [PubMed: 14573951]
24. Terwilliger TC. Automated main-chain model building by template matching and iterative fragment extension. Acta Crystallogr. D Biol. Crystallogr. 2003; 59:38–44. [PubMed: 12499537]
25. McCoy AJ, et al. Phaser crystallographic software. J. Appl. Crystallogr. 2007; 40:658–674. [PubMed: 19461840]
26. Emsley P, Cowtan K. Coot: model-building tools for molecular graphics. Acta Crystallogr. D Biol. Crystallogr. 2004; 60:2126–2132. [PubMed: 15572765]
27. Murshudov GN, Vagin AA, Dodson EJ. Refinement of macromolecular structures by the maximum-likelihood method. Acta Crystallogr. D Biol. Crystallogr. 1997; 53:240–255. [PubMed: 15299926]
28. Brunger AT, et al. Crystallography & NMR system: A new software suite for macromolecular structure determination. Acta Crystallogr. D. 1998; 54:905–921. [PubMed: 9757107]
29. DeLano WL. The PyMOL molecular graphics system. DeLano Scientific, Palo Alto, CA. 2002

30. Dundas J, et al. CASTp: computed atlas of surface topography of proteins with structural and topographical mapping of functionally annotated residues. Nucl. Acids Res. 2006; 34:W116–W118. [PubMed: 16844972]

31. Ho BK, Gruswitz F. HOLLOW: generating accurate representations of channel and interior surfaces in molecular structures. BMC Struct. Biol. 2008; 8:49. [PubMed: 19014592]

32. Laskowski RA, McArthur MW, Moss DS, Thornton JM. PROCHECK: a program to check the quality of protein structures. J. Appl. Crystallogr. 1993; 26:282–291.

33. Lu XJ, Olson WK. 3DNA: a software package for the analysis, rebuilding and visualization of three-dimensional nucleic acid structures. Nucl. Acids Res. 2003; 31:5108–5121. [PubMed: 12930962]

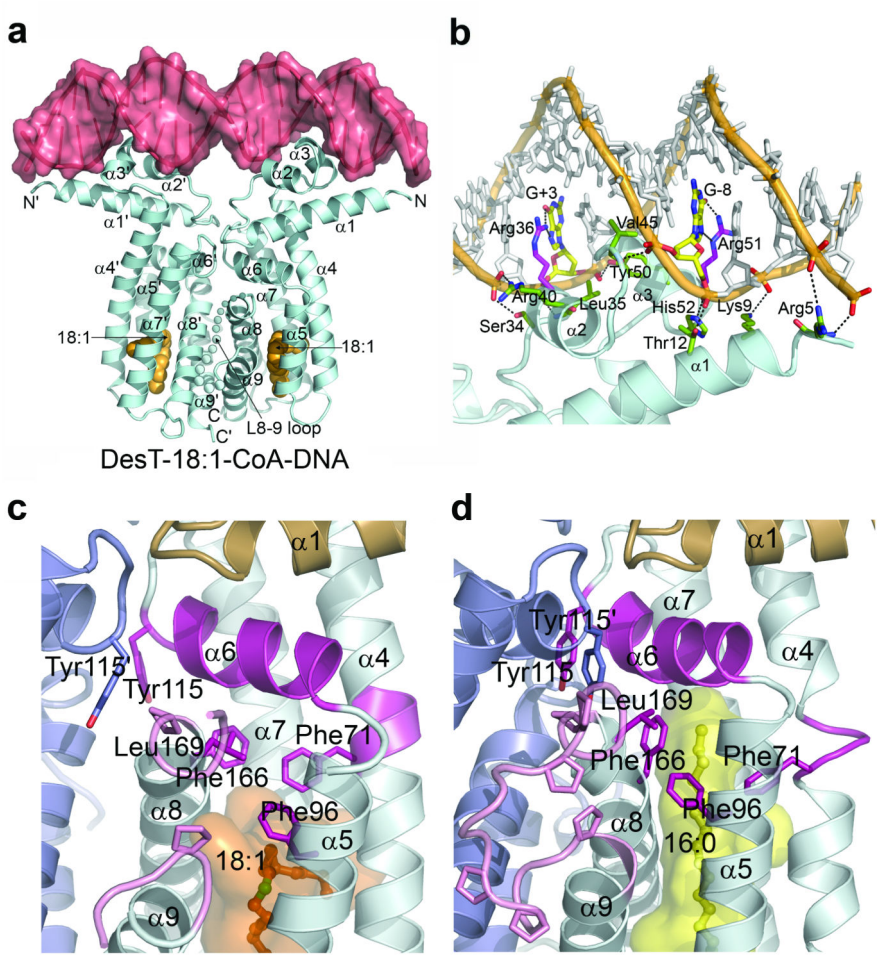

Figure 1. Structural overview of the DesT complexes

(**a**) The DesT–18:1Δ9-CoA–DNA ternary complex. The protein dimer is cyan, the DNA duplex is rose with a semi-transparent surface and the 18:1Δ9 acyl chain is orange CPK. The α-helices and termini are labeled with and without a prime to differentiate the protomers. The L8-9 loop is disordered and shown as a series of spheres. (**b**) Promoter recognition by the DesT DNA-binding domain. Base numbering is with respect to the two-fold symmetry axis of the pseudo palindrome. Protein residues are color-coded according to interaction type: base-specific hydrogen-bonding interactions are magenta, phosphate hydrogen-bonding interactions are green, and van der Waals interactions are orange. The specifically recognized guanines (G+8 and G–3) within the half-site are yellow. (**c**) Relaxed state (DesT–18:1Δ9-CoA–DNA) and (**d**) Tense state (DesT–16:0-CoA) ligand binding cavities. The paired DNA binding domains are brown, and the paired ligand-binding domains are cyan and blue. In the cyan domain, the α4 residues 68 to 71 that partially unwind and helix α6 are both magenta, and the L8-9 loop is pink. 18:1Δ9-CoA and 16:0-CoA and are shown in orange and yellow ball-and-stick, respectively, and the green ball in 18:1Δ9-CoA shows the double bond. Ligand cavity volumes are shown as orange and yellow transparent surfaces. Secondary structure elements and key residues are labeled. The proline-rich interfacial loop L8-9 is disordered in (**c**) but ordered in (**d**).

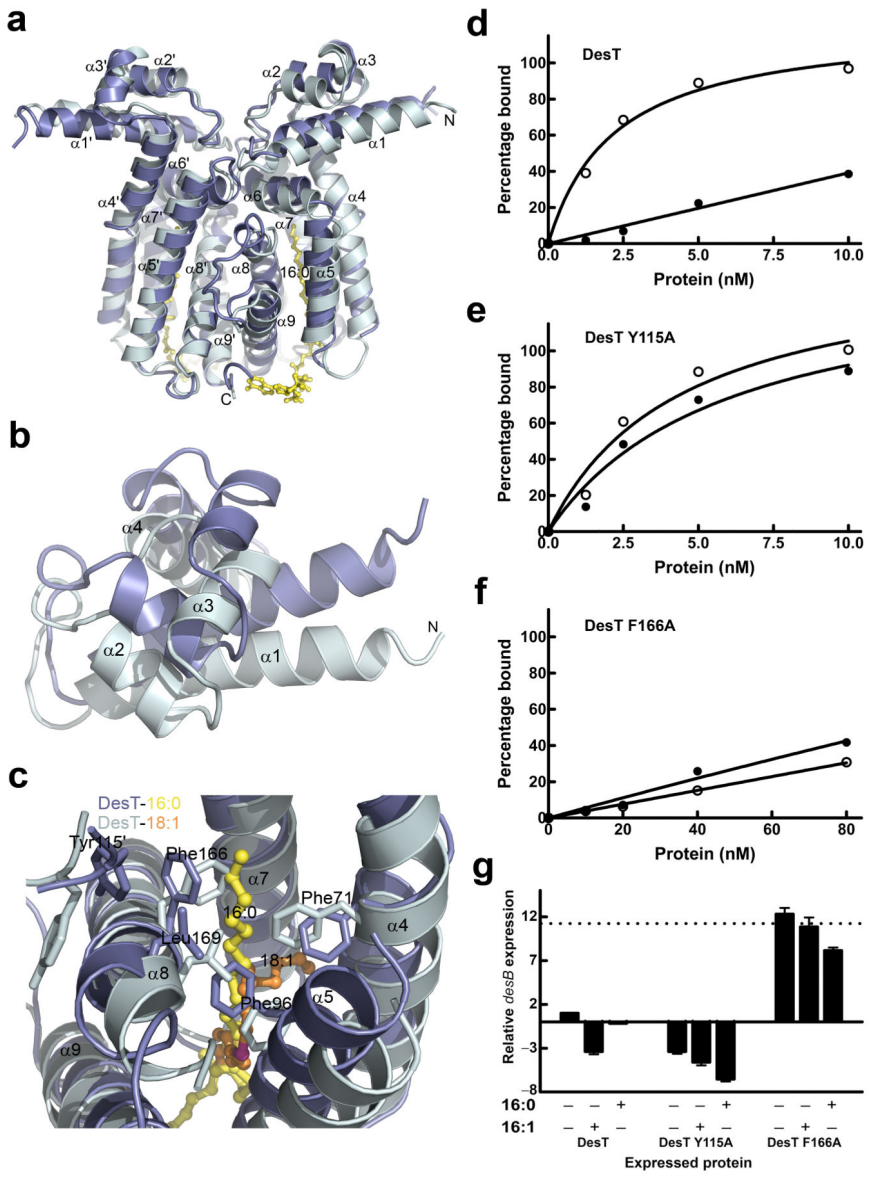

Figure 2. Comparison between the Relaxed (R) and Tense (T) states of DesT, and the allosteric switching mechanism

(**a**) An overlay of the DesT secondary structures in the R (cyan) and T (slate-blue) states with respect to the central four-helical bundle. For reference, the T state ligand (16:0-CoA) is shown in yellow. (**b**) A close up of (**a**) from above showing the DNA-binding domain of one protomer. (**c**) Reorganization of the phenylalanine-rich hydrophobic cluster beneath α6 which has been removed for clarity. The R state side chains and secondary structures are cyan, and the ligand (18:1Δ9-CoA) is orange. The T state side chains and secondary structures are slate-blue, and the ligand (16:0-CoA) is yellow. (**d**), (**e**), (**f**) Ligand-regulated DNA binding of DesT, DesT Y115A and DesT F166A. (**d**) DesT binding to DNA in the presence of either 16:0-CoA (●) or 16:1Δ9-CoA (○). (**e**) DesT Y115A binding to DNA in

the presence of either 16:0-CoA (●) or 16:1Δ9-CoA (○). (**f**) DesT F166A binding to DNA in the presence of either 16:0-CoA (●) or 16:1Δ9-CoA (○). (**g**) Activity of DesT, DesT Y115A and DesT F166A mutants *in vivo*. *P. aeruginosa* strain PA0482 (Δ*desT*) containing an empty expression vector expressed high levels of *desCB* mRNA due to the deletion of the DesT repressor (dotted line). Strain PA0482 derivatives expressing either DesT, or the Y115A or F166A mutants were exposed to either 16:0 or 16:1Δ9. The abundance of *desCB* mRNA was compared by normalizing to the level of mRNA in the strain expressing wild-type DesT in the absence of exogenous fatty acids (set as 1).

Table 1

Data collection and refinement statistics

	18:1Δ9-CoA-DNA (SAD phasing)	18:1Δ9-CoA-DNA	16:0	DNAPP
Data collection				
Space group	$I4_1$	$I4_1$	$P2_1$	$I4_1$
Cell dimensions				
a, *b*, *c* (Å)	78.2, 78.2, 147.4	78.4, 78.4, 148.0	41.7, 100.5, 60.8	79.4, 79.4, 145.5
α, *β*, *γ*, (°)	90, 90, 90	90, 90, 90	90, 105.2, 90	90, 90, 90
Resolution (Å)	3.0(3.1–3.0)*	2.65(2.75–2.65)	2.3(2.4–2.3)	2.5(2.6–2.5)
R_{merge}	11.0(22.9)	7.2(24.8)	5.3(12.5)	4.9(23.1)
$I / \sigma I$	21.3(5.4)	28.4(4.5)	24.4(8.7)	40.4(4.2)
Completeness (%)	91.6(97.7)	98.9(94.6)	98.1(99.9)	96.1(74.5)
Redundancy	4.5(3.9)	7.8(5.3)	3.5(3.5)	7.0(4.6)
Refinement				
Resolution (Å)		30.0–2.65	30.0–2.3	41.0–2.55
No. reflections		12,734	20,078	13,546
R^{work} / R_{free}		22.3/26.1	22.3/27.6	22.8/26.5
No. atoms				
Protein		1481	3145	1470
DNA/acyl-CoA		492/18	0/130	548/0
Water		20	179	15
B-factors				
Protein		70.8	20.1	53.6
DNA/acyl-CoA		106.3/98.7	81.5	82.1
Water		72.8	22.7	51.1
R.m.s. deviations				
Bond lengths (Å)		0.010	0.009	0.010
Bond angles (°)		1.7	1.2	1.4

Each dataset was collected from a single crystal.

*Values in parentheses are for the highest-resolution shell.

Table 2

Acyl-CoA binding and acyl-CoA-dependent DNA binding by DesT and its mutant derivatives.

Protein	Acyl-CoA Binding, Kd [μM][a,b]		DNA Binding, Kd [nM][b,c]			
			1 μM	1 μM	10 μM	10 μM
	16:1-CoA[d]	16:0-CoA	16:1-CoA	16:0-CoA	16:1-CoA	16:0-CoA
DesT	0.93 ± 0.11[e]	2.06 ± 0.30	2.2 ± 0.5	>100	0.9 ± 0.1	>100
DesT Y115A	1.26 ± 0.19	2.34 ± 0.33	4.4 ± 2.0	5.9 ± 2.9	1.7 ± 0.5	4.0 ± 0.4
DesT F166A	3.43 ± 0.71	3.40 ± 0.71	>100	>100	>100	>100
DesT F96A	1.73 ± 0.33	3.39 ± 0.50	3.9 ± 1.0	5.1 ± 0.4	2.7 ± 0.4	7.5 ± 0.8
DesT F71A	3.73 ± 0.38	2.94 ± 0.29	1.7 ± 0.5	1.2 ± 0.4	1.8 ± 0.1	4.0 ± 0.2
DesT L169A	2.11 ± 0.32	1.51 ± 0.17	7.9 ± 0.5	4.8 ± 0.5	8.4 ± 2.6	4.3 ± 0.2

[a] Acyl-CoA dissociation constants were determined using intrinsic protein fluorescence. See Supplementary Figs. 4a & 4b for examples of the fluorescence titration experiments.

[b] The binding constants were determined using non-linear regression to fit the data to a one-site binding model with Graphpad software.

[c] DNA binding was measured using the electrophoretic gel shift assay. See Supplementary Figs. 4c & 4d for examples of the gel shift assays.

[d] 16:0-CoA and 16:1Δ9-CoA were used to compare acyl chains with the same number of carbon atoms.

[e] mean ± s.d.